Atmospheric Research 113 (2012) 113–125

Contents lists available at SciVerse ScienceDirect

Atmospheric Research

journal homepage: www.elsevier.com/locate/atmos

Comparison of optical properties of nitrate and sulfate aerosol and the direct radiative forcing due to nitrate in China

H. Zhang [a,*], Z. Shen [a,b], X. Wei [a,c], M. Zhang [d], Z. Li [e,f]

[a] Laboratory for Climate Studies, National Climate Center, China Meteorological Administration, Beijing 100081, China
[b] Shanghai Climate Center, Shanghai, China
[c] Graduate University of Chinese Academy of Sciences, Beijing, China
[d] State Key Laboratory of Atmospheric Boundary Layer Physics and Atmospheric Chemistry, Institute of Atmospheric Physics, Chinese Academy of Sciences, Beijing 100029, China
[e] Dept. of Atmos. & Oceanic Sci., UMCP, MD, USA
[f] SLESPRE/GCESS, Beijing Normal University, Beijing, China

ARTICLE INFO

Article history:
Received 1 June 2011
Received in revised form 25 April 2012
Accepted 27 April 2012

Keywords:
Nitrate aerosol
Optical property
Direct radiative forcing
Sulfate aerosol
China region

ABSTRACT

In previous studies, the optical properties of sulfate aerosols were employed to estimate the direct radiative forcing (DRF) due to nitrate aerosols. Ensuing errors have not been rigorously evaluated, which is a major objective of this study. First, we compared the optical properties of nitrate and sulfate aerosols in different spectral regions. Our results show that nitrate is a strongly scattering aerosol and in some spectral regions, its scattering properties are even greater than those of sulfate aerosols. For example, nitrate aerosol single-scattering albedos are about 40% greater than those of sulfates when the wavelength is nearly 2.8 μm and the relative humidity (RH) is below 40%. We then incorporated the optical parameters of nitrate into a radiative transfer model and estimated the DRF due to nitrate aerosols at the top of the atmosphere (TOA) under both clear- and all-sky conditions and compared them with those of sulfate aerosols. We found that the local forcing due to nitrate aerosols using sulfate optical properties in the simulation can be underestimated by a maximum of 6.2% under all-sky conditions.

Using model-simulated nitrate concentrations in China that reproduce observed features reasonably well, we found significant spatial and seasonal changes in DRFs due to nitrate aerosols. DRFs were stronger in winter, spring, and autumn, but much weaker in summer. The annual mean values of the forcings over China were $-4.51\ \mathrm{W\ m^{-2}}$ and $-0.95\ \mathrm{W\ m^{-2}}$ under clear-sky and all-sky conditions, respectively. Clouds play an important role in determining the DRF and can greatly reduce the forcing strength and its geographical extent.

1. Introduction

Inorganic nitrates, in either pure or mixed forms, frequently constitute a major fraction of ambient aerosols. They belong to a family of secondary aerosols and are mainly transformed from nitrogen oxide. The Fourth Assessment Report of the Intergovernmental Panel on Climate Change (IPCC, 2007) estimated a large, global, fine-mode nitrate burden of 0.58 mg $NO_3\ m^{-2}$, which would imply an equivalent of 20% of the mean anthropogenic sulfate burden. Furthermore, surface observations of fine-mode nitrate particles show that high concentrations are mainly found in highly industrialized regions, while low concentrations are found in rural areas.

Nitrate is a major type of anthropogenic aerosol. Like sulfate aerosols, nitrate aerosols can also have a significant impact on Earth's climate. Although some studies have investigated the radiative forcings due to sulfate and nitrate aerosols and their climatic effects (Wang et al., 2003, 2010; Pham et al., 2005; Quinn and Bates, 2005; Dentener et al., 2006; Li et al., 2009), few studies have focused on the differences in optical properties

* Corresponding author.
E-mail address: huazhang@cma.gov.cn (H. Zhang).

0169-8095/$ – see front matter © 2012 Elsevier B.V. All rights reserved.
doi:10.1016/j.atmosres.2012.04.020

between nitrate and sulfate aerosols, and about the discrepancies in direct radiative forcing (DRF) calculations brought on by these differences, especially in large emission regions.

Over the period of 1979–1981, Diederen et al. (1985) measured the scattering properties of different aerosols in The Netherlands and found that other aerosol components were as important as sulfates in terms of scattering properties. In particular, nitrates, while present in lower quantities than sulfates, appeared to contribute equally to aerosol scattering (Ten Brink et al., 1996). Bergin et al. (2001) found that nitrates contributed 8% toward the PM2.5 chemical composition in Beijing and nitrate formation may contribute to the observed peaks in total aerosol extinction and single-scattering albedo in Beijing. For the A2 emission scenario of the IPCC's Special Report on Emissions Scenarios (SRES), Adams et al. (2001) and Liao et al. (2004) used the Goddard Institute for Space Studies general circulation model II-prime (GISS GCM II) to estimate the current and 2100 global mean DRF due to nitrate and sulfate aerosols. Their results suggested that although the DRF due to anthropogenic sulfate aerosols would decrease in the future, forcing due to anthropogenic nitrate aerosols would increase over the next 100 years, significantly exceeding that of sulfate aerosols. Van Dorland et al. (1997) used a broadband radiative transfer model to investigate the DRF of nitrate aerosols over the period of 1850–1990. The global mean DRF due to nitrate aerosols was $-0.03\ \mathrm{W\ m^{-2}}$; the maximum value of $-0.4\ \mathrm{W\ m^{-2}}$ occurred in January over southeastern Asia. It was pointed out in the IPCC report (2007) that the estimated global mean DRF at the top of the atmosphere (TOA) due to nitrate aerosols was in the range of $-0.10 \pm 0.10\ \mathrm{W\ m^{-2}}$. The uncertainty in the estimation was large, owing to the relatively small number of studies. The radiative forcing of nitrate aerosols on hemispheric and global scales may not be very significant, but over China, this forcing can be much more important because of the magnitude of emissions there (Li et al., 2007).

The DRF due to nitrate aerosols is sensitive to atmospheric concentrations of nitrogen oxide from emissions (IPCC, 2007). Nitrogen oxide emissions from fossil fuel combustion and vehicle exhaust have increased rapidly in China over the past three decades because of the rapid economic development in that part of the world (Streets and Waldhoff, 2000; Ohara et al., 2007). This would suggest that the proportion of nitrate aerosols in the atmosphere has also greatly increased. This realization sparked research into the climate effects of nitrate aerosols (An et al., 2002; Liao and Seinfeld, 2005; Wang et al., 2010). Van Dorland et al. (1997) used the optical properties of sulfate aerosols at 80% RH to estimate the nitrate DRF. Adams et al. (2001) ignored the imaginary part of refractive indices of nitrate aerosols and used only their real refractive indices at 0.58 μm (Tang, 1996). Liao et al. (2004) used the optical properties of sulfate aerosols to calculate the nitrate DRF; Wang et al. (2010) multiplied a factor with the optical depth of sulfate aerosols to estimate the nitrate DRF. No studies to date have examined the DRF due to nitrate aerosols in China using nitrate optical properties. The treatment of nitrate aerosols is still much more rudimentary than sulfate aerosols. In this work, nitrate optical properties are calculated accurately using the refractive index from the HITRAN 2004 database (Rothman et al., 2005). The uncertainty of refractive indices in the HITRAN database is less than 5% (e.g., Myhre et al., 2005).

In this study, we first compare the optical properties of nitrates with those of sulfates, then calculate the DRF due to nitrate aerosols over China, using its own optical properties. We evaluate the errors produced by using the optical properties of sulfate aerosols to estimate the DRF due to nitrate aerosols. The radiative transfer model and input datasets used are described in Section 2. Section 3 presents the detailed analysis and discussion, and Section 4 gives a summary.

2. Radiative transfer model and aerosol dataset

2.1. Model description

We used the radiative transfer model developed at the Beijing Climate Center (RAD_BCC), which was improved by Zhang et al. (2006a, 2006b, 2009) on the basis of the BSTAR5C and MSTRNX models (see http://www.ccsr.u-tokyo.ac.jp/~clastr/index.html for details). The algorithm proposed by Nakajima et al. (2000) is used to treat clouds and aerosols, and the algorithm by Zhang et al. (2003) is adopted for greenhouse gases. The 10–49000 $\mathrm{cm^{-1}}$ spectral range was divided into 17 bands (8 longwave and 9 shortwave), which includes six major greenhouse gases in each band: H_2O, CO_2, O_3, N_2O, CH_4, and CFCs. The O_2 and O_3 continuum absorptions were also considered in the shortwave region. We only consider the effects of nitrate aerosols in the solar region. Table 1 lists the band divisions that were used in this study.

2.2. Aerosol dataset and the DRF calculation method

First, we calculated the extinction coefficient, single-scattering albedo, and asymmetry factor of nitrate and sulfate aerosols according to the Mie theory for spherical particles and complex refractive indices from the updated HITRAN 2004 database (Rothman et al., 2005) and Mie code (Wiscombe, 1980).

The lognormal distribution (WMO, 1983) is employed in this study:

$$n(\mathrm{r}) = \frac{dN(\mathrm{r})}{dr} = \frac{\mathrm{N_0}}{\mathrm{r}\sigma\sqrt{2\pi}} \cdot \exp\left[-\frac{(\ln \mathrm{r} - \ln \mathrm{r_m})^2}{2\sigma^2}\right], \quad (1)$$

where $\mathrm{r_m}$ and σ are the mode radius and standard deviation, respectively, and $\mathrm{N_0}$ is the number density of nitrate aerosols. The size distribution of nitrate aerosols is divided into the nucleus mode and the accumulation mode. For the nucleus mode, $\mathrm{r_m}$ and σ are equal to 0.015 μm and 1.7, respectively;

Table 1
Description of shortwave band divisions.

Band	Wavelength (μm)	Absorption gases, aerosol, cloud
9	1.923–3.731	H_2O, aerosol, cloud
10	0.833–1.923	H_2O, aerosol, cloud
11	0.455–0.833	H_2O, O_3, aerosol, cloud
12	0.323–0.455	Rayleigh scattering, aerosol, cloud
13	0.303–0.323	O_3, aerosol, cloud
14	0.286–0.303	O_3, aerosol, cloud
15	0.270–0.286	O_3, aerosol, cloud
16	0.233–0.270	O_3, O_2, aerosol, cloud
17	0.204–0.233	O_3, O_2, aerosol, cloud

for the accumulation mode, r_m and σ are equal to 0.15 μm and 1.9, respectively. The volume concentrations of the nucleus mode and the accumulation mode are 1% and 99%, respectively. These size distribution parameters were used previously to calculate the aerosol optical depth (AOD) over East Asia. Simulated total AOD with nitrate aerosols included can reproduce observed temporal and spatial features very well over East Asia (Han et al., 2010). The nitrate aerosol size distribution used in this paper is also consistent with observations made by Sun et al. (2010) and Zhang et al. (2011) in Beijing. Nitrate and sulfate aerosols are both water absorbing aerosols, so the size distribution and refractive index are different at different RH levels. In this work, the mode radius in the size distribution at different RHs are calculated according to the Kohler equation, while refractive indices at different RHs are calculated by weighting the volume ratio of aerosols to that of liquid water, i.e., assuming external mixing.

For a given size distribution, the bulk single-scattering properties (SSPs) of aerosols include the mean extinction efficiency (Q_e), the single scattering albedo (ω), and the scattering phase function (P_{11}). These quantities can be written as follows:

$$Q_e = \frac{\int_{r_{min}}^{r_{max}} Q_e'(r)S(r)n(r)dr}{\int_{r_{min}}^{r_{max}} S(r)n(r)dr}, \quad (2)$$

$$\omega = \frac{\int_{r_{min}}^{r_{max}} Q_s'(r)S(r)n(r)dr}{\int_{r_{min}}^{r_{max}} Q_e'(r)S(r)n(r)dr}, \quad (3)$$

$$P_{11} = \frac{\int_{r_{min}}^{r_{max}} P_{11}'(r)Q_s'(r)S(r)n(r)dr}{\int_{r_{min}}^{r_{max}} Q_s'(r)S(r)n(r)dr}, \quad (4)$$

where r, Q_e, Q_s, P_{11} and S are the particle radius, extinction and scattering efficiencies, the scattering phase function and the projected area, respectively, for an individual particle. The asymmetry factor (g) indicates the relative intensity of forward and backward scattering and is a key input parameter for a radiative transfer model. It can be written as:

$$g = \frac{1}{2}\int_{-1}^{1} P_{11}(\cos\Theta)\cos\Theta d\cos\Theta, \quad (5)$$

where Θ is the scattering angle.

Nitrate aerosol concentrations were simulated by the Community Multi-scale Air Quality Modeling System (CMAQ) coupled with the Regional Air Modeling System (RAMS). Their horizontal resolution is 81 km × 81 km, while in the vertical, there are 23 layers in the σ_Z coordinates system, unequally spaced from the ground to ~23 km, with about 9 layers concentrated in the lowest 2 km of the atmosphere (Zhang et al., 2007). A comparison of simulated and modeled nitrate aerosol concentrations over East Asia during the Transport and Chemical Evolution over the Pacific (TRACE-P) shows that the model reproduced observed features reasonably well (see Zhang et al. (2007) for details). Therefore in this study, we use the monthly mean concentration of nitrate aerosol output from the model system and the corresponding meteorological field profiles (e.g., temperature, pressure, and specific humidity) for the year 2005.

Surface albedo and ozone column burdens over China were obtained from the International Satellite Cloud Climatology Project-Flux Data product (ISCCP-FD; ftp://isccp.giss.nasa.gov/outgoing/FLUX). Vertical profiles of ozone concentration were calculated from the ozone column burdens using an empirical formula proposed by Lacis and Hansen (1974). Water vapor concentrations were converted from specific humidity. The concentration of O_2 is assumed to be evenly mixed in the atmosphere and is set at 209,000 ppmv.

From the ISCCP D2 dataset with a global grid resolution of 2.5° × 2.5° (Rossow and Schiffer, 1999; Schiffer and Rossow, 1983), we used the cloud optical thickness, cloud-top pressure, cloud cover (C), and cloud water/ice path (WP; LWP and IWP for liquid and ice water paths, respectively) of 15 cloud categories at different cloud phases. Low, middle, and high clouds were added between 1000 and 680 mb, 680 and 440 mb, and 440 and 50 mb, respectively. The barometric height formula was used to calculate the geometric thickness of clouds (Δz). The water content (WC) of liquid and ice clouds is given by

$$WC = WP/\Delta z. \quad (6)$$

The cloud droplet effective radius, r_e, is approximated as:

$$r_e \approx \frac{3}{2\rho_{cloud}}\frac{WP}{\tau_{cloud}}, \quad (7)$$

where ρ_{cloud} is the water (or ice) density and τ_{cloud} is the optical depth of the cloud.

These cloud parameters (cloud water content, cloud droplet effective radius, and cloud geometric thickness) were incorporated into the RAD_BCC to calculate the DRF for an overcast sky. The following formula was used to calculate the instantaneous DRF at the TOA due to nitrate aerosols under overcast sky conditions:

$$DRF_{TOA} = \Delta F_{TOA}(NO_3 + cloud) - \Delta F_{TOA}(cloud), \quad (8)$$

where "NO_3 + cloud" represents an atmosphere containing nitrate aerosols and clouds, "cloud" indicates a cloudy atmosphere without nitrate aerosols, and ΔF_{TOA} is the net solar radiative flux at the TOA. We first calculated net solar radiative fluxes at the TOA for an overcast sky case, with both nitrate aerosols and clouds included in the model simulation. Then we removed nitrate aerosols, while keeping all other conditions the same, and recalculated net solar radiative fluxes at the TOA. The difference between the two results, as in Eq. (8), is the instantaneous DRF due to nitrate aerosols. Clear-sky calculations are made without including clouds in Eq. (8).

To calculate the DRF for an all-sky case, we modified the method of Yang et al. (2008) by substituting the DRF into their heating rate formulation:

$$RF = \sum_{i=1}^{15} C_i RF_i + (1-C)RF_{clear}, \quad (9)$$

where C_i is the cloud cover in each cloud category, $C = \sum_{i=1}^{15} C_i$ is the total cloud cover, and RF_{clear}, RF_i, and RF are the radiative

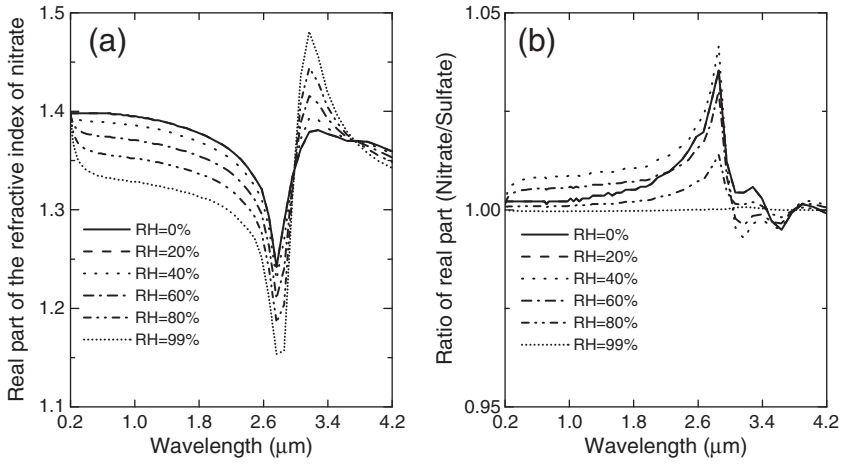

Fig. 1. Real part of the refractive index of nitrate as a function of wavelength (a) and the nitrate-to-sulfate ratio of the real parts of their refractive indices as a function of wavelength (b) for different RH values.

forcings of clear-, cloudy- (cloud category: i), and all-sky cases, respectively.

The daily averaged shortwave radiative forcing (SWARF) due to nitrate aerosols was calculated using the scheme of Liu et al. (2003):

$$SWARF = \frac{1}{n}\sum_{i=1}^{n} \frac{\frac{1}{24}\int_{\text{sunrise}}^{\text{sunset}} (\sin\varphi\sin\delta + \cos\varphi\cos\delta\cos H)dH}{(\sin\varphi\sin\delta + \cos\varphi\cos\delta\cos H_i)} ISWARF(H_i), \tag{10}$$

where $ISWARF(H_i)$ is the instantaneous DRF at hour angle H_i, n is the number of hour angles, and φ and δ are latitude and declination angles, respectively. Using a first-order approximation (i.e., n = 1), we assume that

$$\sin\phi\sin\delta + \cos\varphi\cos\delta\cos H_1 = \frac{1}{24}\int_{\text{sunrise}}^{\text{sunset}} (\sin\varphi\sin\delta + \cos\varphi\cos\delta\cos H)dH. \tag{11}$$

Then $SWARF = ISWARF(H_1)$, where the hour angle H_1 must satisfy Eq. (11).

3. Results

3.1. Optical property comparisons between nitrate and sulfate aerosols

The refractive index is a key parameter in determining the scattering and absorption characteristics of aerosols. It consists of real and imaginary parts that indicate the relative intensity of scattering and absorption, respectively. The DRF due to aerosols can be positive or negative, depending mainly on the magnitude of the imaginary part of the refractive index (Yamamoto and Tanaka, 1971). Fig. 1 shows the real part of the nitrate refractive index and the ratio of the real

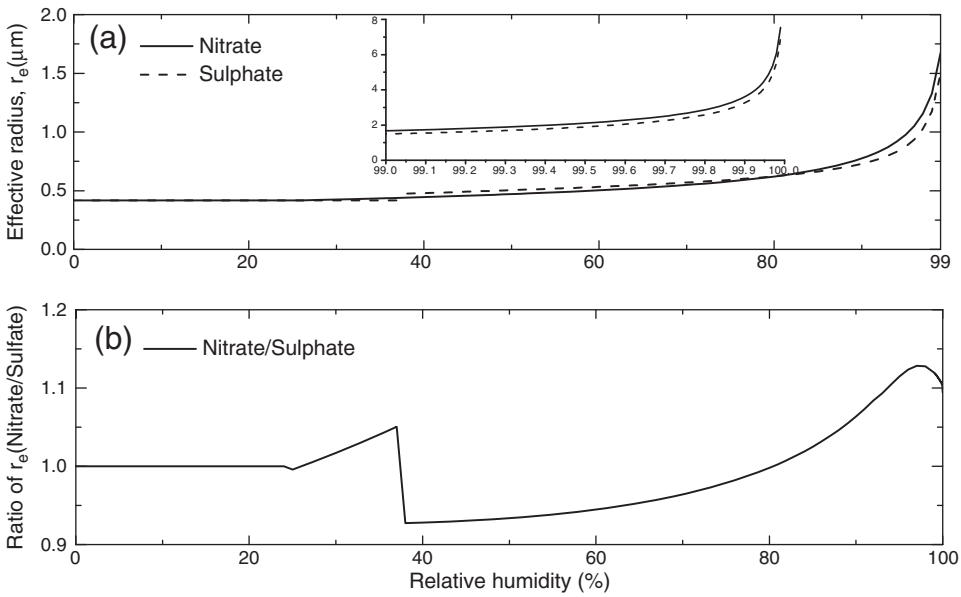

Fig. 2. Effective radii of nitrate and sulfate as a function of RH (a) and the nitrate-to-sulfate ratio of their effective radii as a function of RH (b).

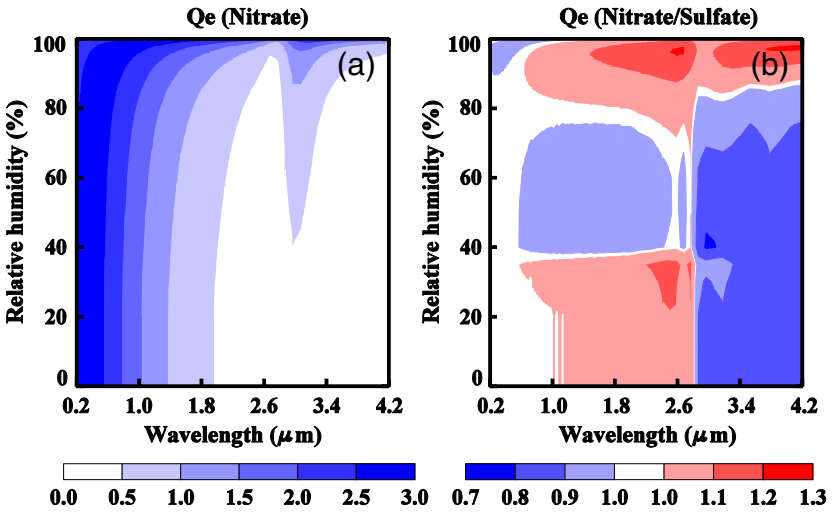

Fig. 3. Extinction efficiency factor of nitrate (a) and the nitrate-to-sulfate ratio of their extinction efficiency factors (b) as a function of RH and wavelength.

part of the refractive index of nitrate to that of sulfate as a function of wavelength for different RH levels. As illustrated in Fig. 1a, the solid line and the dashed line (the real parts of the refractive index at RH = 0% and 20%, respectively) overlap throughout the whole solar spectral region. The real part of the refractive index increases with increasing RH (for RH > 20%) when the wavelength ranges from 2.8 to 3.3 μm and decreases with increasing RH (for RH > 20%) in the other solar bands. Minimum and maximum values for the real part of the refractive index at all RH levels occur at around 2.8 μm and 3.3 μm, respectively. Fig. 1b shows that differences in the real parts of the refractive index for nitrates and sulfates become smaller with increasing RH throughout the whole solar spectral region until they converge when RH reaches 99%. The nitrate-to-sulfate ratio of the real part of the refractive index increases with increasing wavelength for wavelengths less than 2.8 μm. A peak in the magnitude of the ratios at all RH levels occurs at 2.8 μm, where a maximum value of 1.04 is reached at RH = 40%. When the wavelength is greater than 2.8 μm, differences between the ratios at all RH levels are small.

Fig. 2(a) and (b) shows the effective radius (r_e) of nitrate and sulfate aerosols and their ratio as a function of RH, respectively. The r_e of both aerosols is equal when the RH is less than 20%. At RH levels ranging from 37% to 80%, the r_e of nitrate is smaller than that of sulfate; outside this range (20%–37% and 80%–100%), the r_e of nitrate is greater than that of sulfate. When RH is less than 37%, relative differences in r_e between nitrates and sulfates are under 5%; when RH is between 37% and 80%, relative differences are larger than 5%. Relative differences increase rapidly once RH levels greater than 80% are reached; at RH = 97%, relative differences are at a maximum value of 13%.

The extinction efficiency factor (Q_e) should be closely related to refractive index and size distribution. Fig. 3 shows the change in Q_e of nitrate and the nitrate-to-sulfate ratio of Q_e at different RH levels. Q_e decreases as wavelength increases (Fig. 3a) but the change in Q_e with RH is not obvious. The value

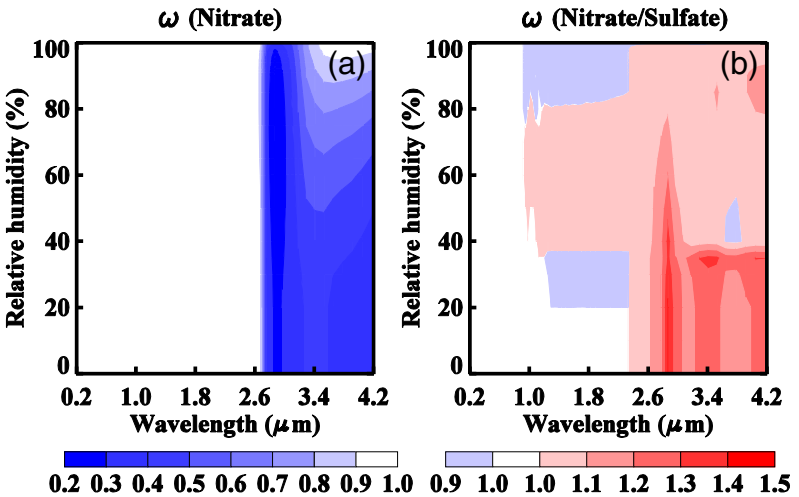

Fig. 4. Same as Fig. 3, but for the single scattering albedo.

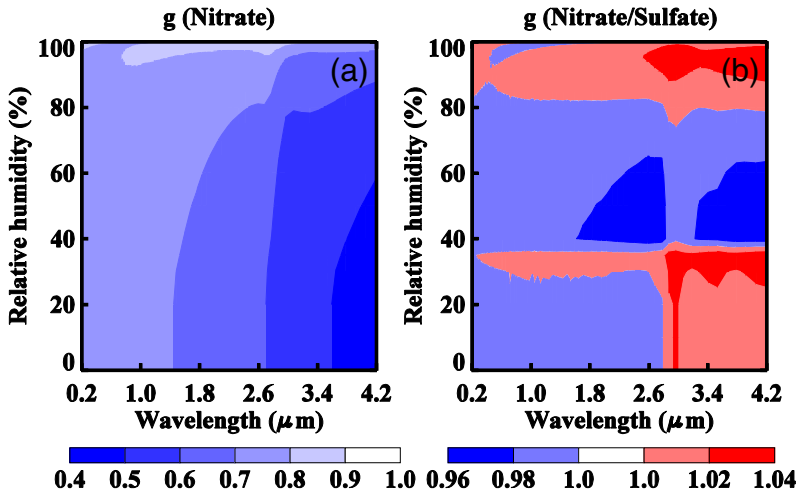

Fig. 5. Same as Fig. 3, but for the asymmetry factor.

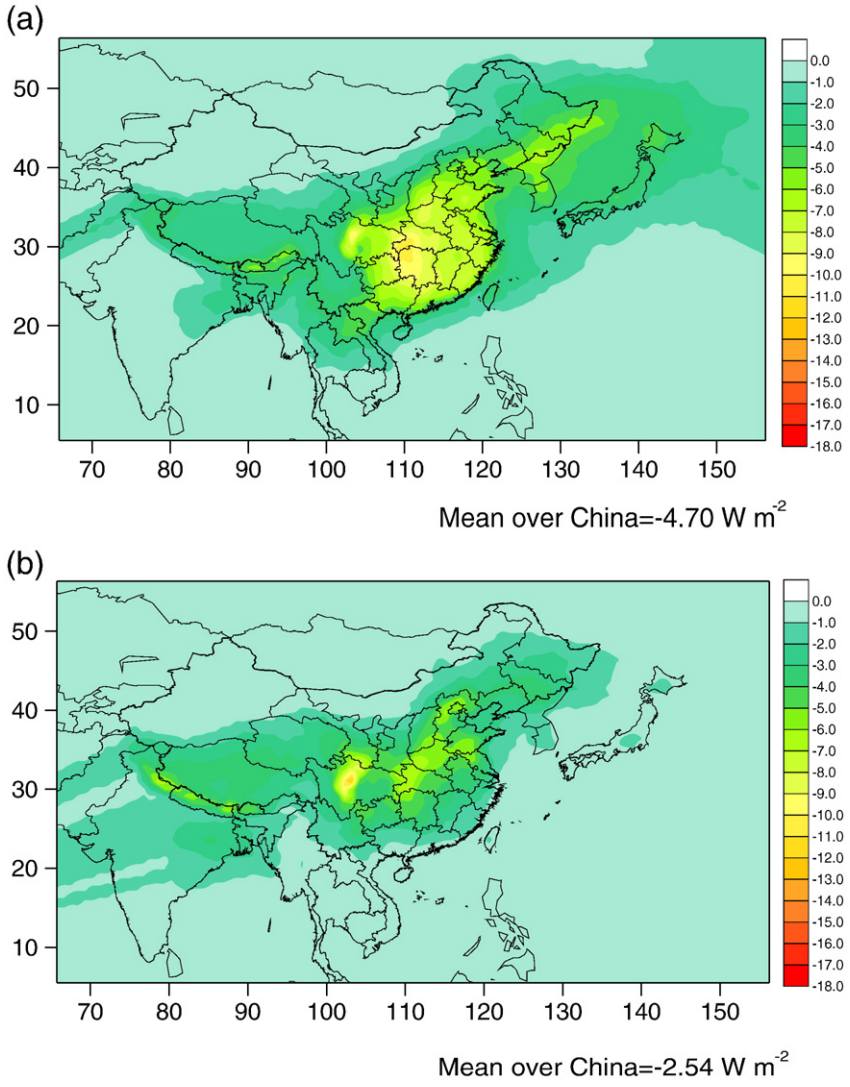

Fig. 6. Distribution of mean direct radiative forcing (W m^{-2}) due to nitrate aerosols at the TOA under clear-sky (left panels) and all-sky (right panels) conditions in (a) spring, (b) summer, (c) autumn, and (d) winter.

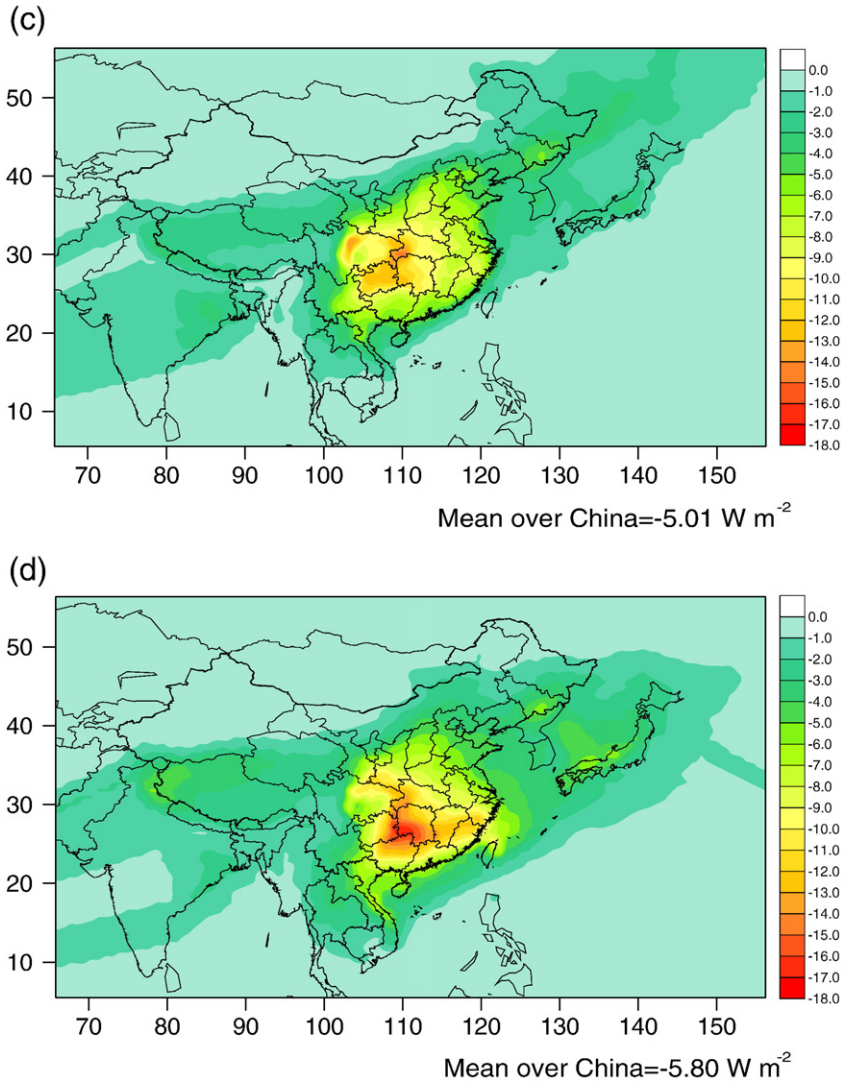

Fig. 6 (*continued*).

of Q_e between 0.2 and 0.8 μm at all RH levels is larger than 2.0 and the value of Q_e between 2.0 and 4.2 μm at all RHs is smaller than 0.5 except near 2.8 μm (RH = 40%). When RH is less than 37% and the wavelength is less than 2.8 μm, the extinction efficiency of nitrate is larger than that of sulfate (see Fig. 3b); if the wavelength is greater than 2.8 μm, the reverse is seen. This is mainly due to the difference in refractive indices of both aerosols at wavelengths less than and greater than 2.8 μm (see Fig. 1b). When RH is greater than 37%, the difference between the extinction efficiencies of nitrate and sulfate is mainly attributed to obvious differences existing in the magnitude of their respective r_e (i.e., the size distribution) shown in Fig. 2. When RH ranges from 37 to 80%, the extinction efficiency of nitrate is smaller than that of sulfate because the effective radius of nitrate is smaller than that of sulfate (see Fig. 2a); the converse is true for RH greater than 80%.

Fig. 4 shows how the single-scattering albedo (ω) of nitrate and the nitrate-to-sulfate ratio of ω changes with wavelength and RH. A minimum in ω is seen at around 2.8 μm at all RH levels, and as RH increases, ω increases because of hygroscopic growth (Fig. 4a). Fig. 4b shows that there are significant differences in ω for nitrates and sulfates at specific wavelengths. For example, when the wavelength is nearly 2.8 μm and the RH is below 40%, the ω for nitrates are about 40% greater than those for sulfates, which can also be explained by differences in their refractive indices at 2.8 μm (see Fig. 1b).

Fig. 5 is the same as Fig. 4, but for the asymmetry factor. The asymmetry factor of nitrate decreases as the wavelength increases because the scattering approaches Rayleigh scattering with increasing wavelength. Fig. 5b illustrates that differences in asymmetry factor between nitrates and sulfates are relatively small, with relative differences under ±4%.

The optical properties of nitrate and sulfate shown here suggest that the differences in Q_e and ω between them are large in some spectral regions and under some RH conditions. Therefore, use of optical properties of sulfate aerosols when

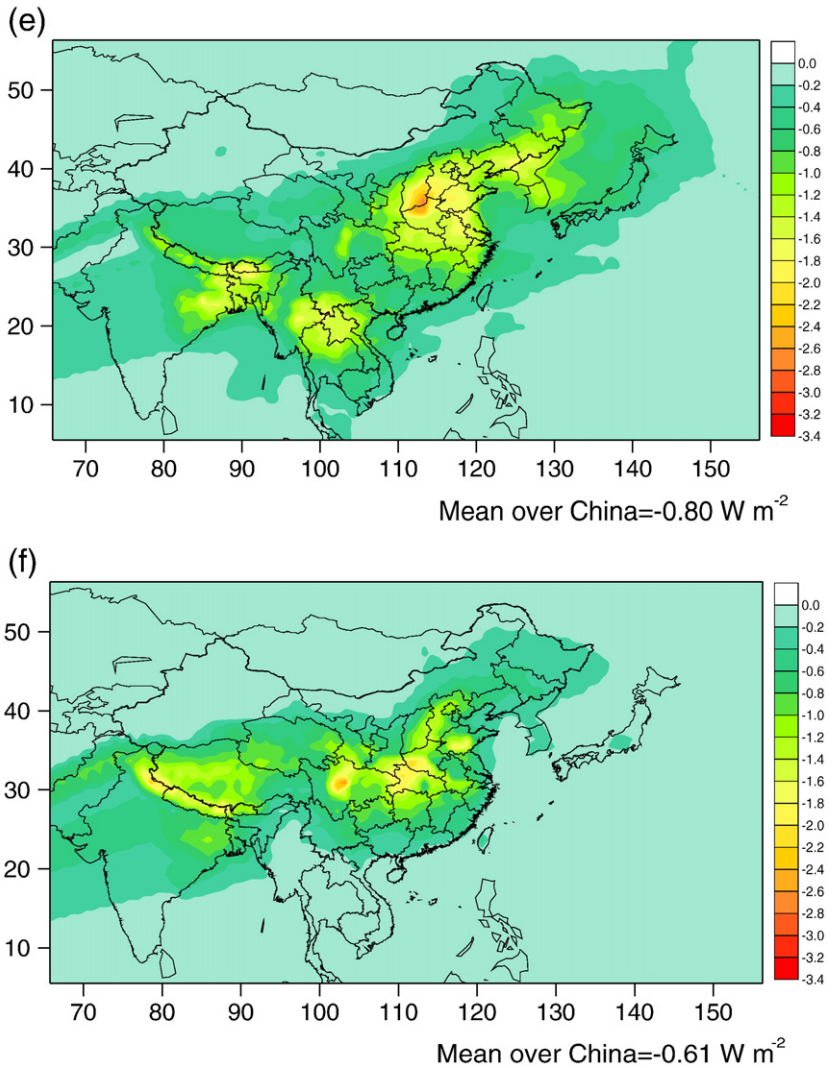

Fig. 6 (*continued*).

calculating the DRF due to nitrate aerosols may lead to uncertainties, which will be evaluated Section 3.4.

3.2. The distribution of seasonal mean DRF due to nitrate aerosols in China

Nitrate aerosols strongly scatter solar radiation, which leads to a negative forcing at the TOA. Fig. 6 shows the geographical distribution of the seasonal mean DRF due to nitrate aerosols under clear-sky (a–d) and all-sky (e–h) conditions. In spring, nitrate aerosol DRFs were mainly distributed over central, east, and northeast China, attaining a maximum value of $-2.70\,W\,m^{-2}$ for the all-sky case. Mean all-sky DRFs over southern China were significantly lower ($-0.58\,W\,m^{-2}$) compared to mean clear-sky DRFs ($-5.17\,W\,m^{-2}$), a nearly ninefold reduction in absolute value, mainly because of the large cloud cover (>90%) over this region during springtime. Moreover, forcings were also largely reduced over the adjacent seas, including the Bo Sea (Bohai), the Yellow Sea, and the Japan/East Sea. The lowest DRFs were seen during the summer in both clear- and all-sky cases (Fig. 6b and f), with seasonal mean values of $-2.54\,W\,m^{-2}$ and $-0.61\,W\,m^{-2}$, respectively. There is more precipitation during the summer so stronger wet scavenging of aerosols occurs, leading to smaller DRFs for the all-sky case. The higher temperatures during the summer are also not favorable to the formation of nitrate aerosols. In the autumn, forcings were mainly distributed throughout central and southeast China, with a maximum value of $-2.81\,W\,m^{-2}$ for the all-sky case (Fig. 6g). The seasonal mean DRF of nitrate aerosols was the greatest in winter under clear-sky conditions and in autumn under all-sky conditions when cloud cover is at a minimum. In winter, a maximum forcing of $-3.83\,W\,m^{-2}$ occurred in central China under all-sky conditions. The smallest forcings were located over southeast China, due to cloud cover, which was usually more than 90%, whereas forcings in the eastern coastal region of India and northwest Thailand, which had less cloud cover,

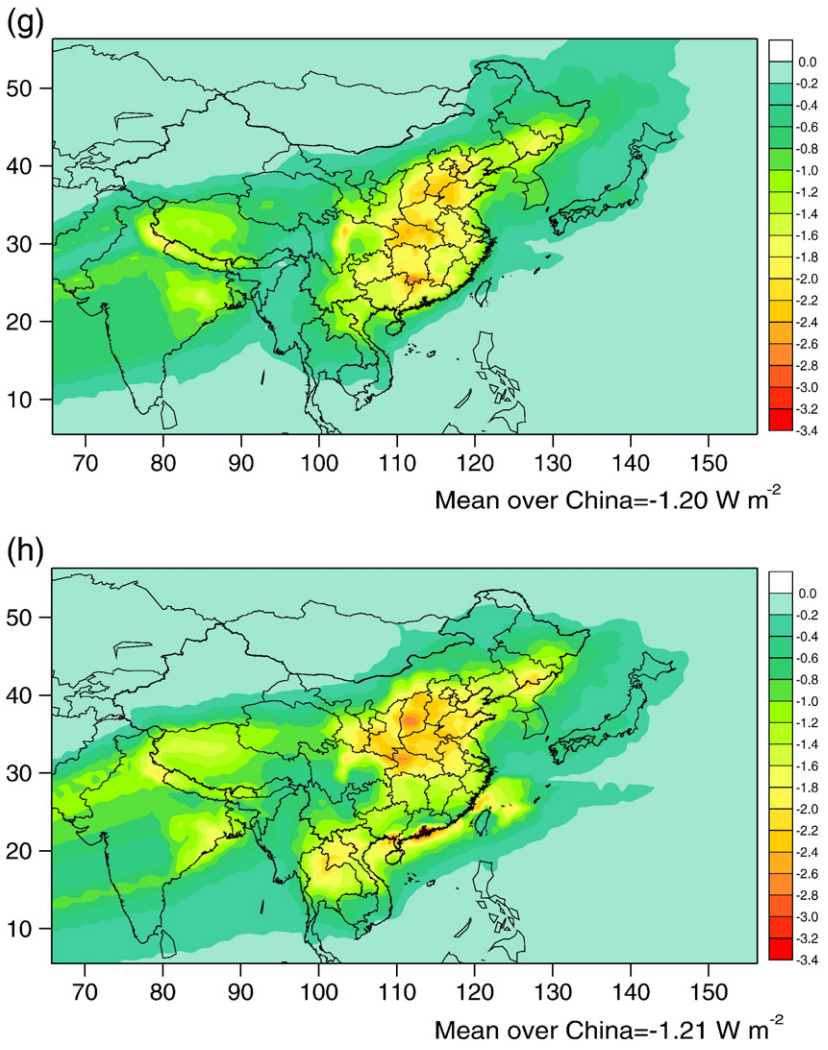

Fig. 6 (*continued*).

were much higher. The seasonal mean DRFs under all-sky conditions over China in spring, summer, autumn, and winter were 82.98%, 75.98%, 76.05%, and 79.14% less than those under clear-sky conditions, respectively.

Cloud cover greatly affects the DRF and can significantly reduce the strength and range of forcings. Areas with the greatest magnitudes of DRF under all-sky conditions coincided with those under clear-sky conditions. However, differences did arise in some regions. The range of values for the DRF over the sea in summer and autumn were significantly less than those in winter and spring. This is probably related to changes in the prevailing weather systems over sea and land and the adjustment of the land–sea breeze in East Asia in different seasons. In summer and autumn, wind mainly blows from the sea to the land in the lower atmosphere, leading to a decrease in nitrate aerosol loading over the sea. In winter and spring, the wind direction reverses and nitrate aerosols can be transported far away over the sea.

Fig. 7 shows the geographical distribution of the annual mean all-sky forcing of nitrate aerosols over China; the annual mean DRF was $-0.95\ \mathrm{W\ m^{-2}}$. Large forcings were mainly distributed over central China, which is consistent with the result of Liao and Seinfeld (2005), although the maximum value ($-2.17\ \mathrm{W\ m^{-2}}$) is somewhat smaller than what they reported ($-3.00\ \mathrm{W\ m^{-2}}$).

3.3. Comparison of monthly mean DRFs in different regions of China

Because human activities and industrialization vary greatly in different areas of China, and nitrate aerosols are mainly produced by these activities, there are distinct regional differences in local nitrate aerosol emissions. Table 2 lists the monthly and annual mean DRFs in different regions of China under clear-sky and all-sky conditions.

In the all-sky case, forcing values for all months and regions were lower than those under clear-sky conditions by varying

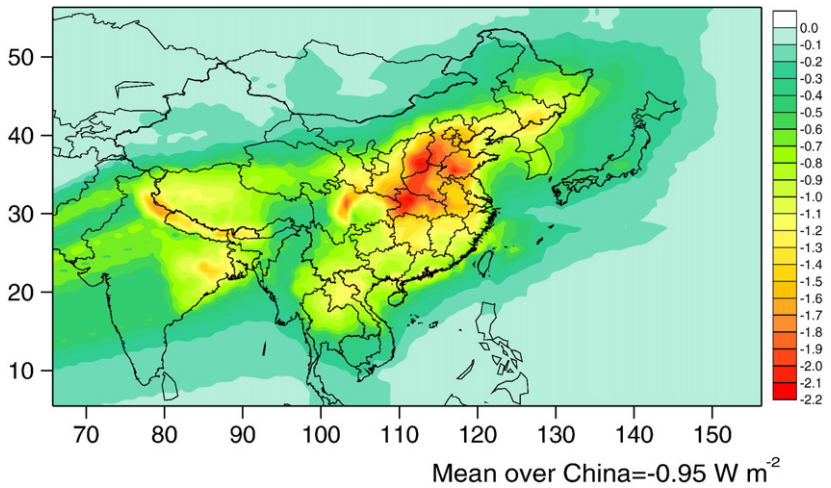

Fig. 7. Distribution of annual mean direct radiative forcing ($W\,m^{-2}$) due to nitrate aerosols at the TOA under all-sky conditions.

amounts. Annual mean DRFs in central and east China were largest under both clear- and all-sky conditions, with clear-sky values of -8.53 and $-5.92\ W\,m^{-2}$, respectively, and all-sky values of -1.57 and $-1.14\ W\,m^{-2}$, respectively. The smallest annual mean clear-sky DRF occurred in northeast China, with a value of $-2.14\ W\,m^{-2}$, whereas the all-sky minimum occurred in northwest China, with a value of $-0.53\ W\,m^{-2}$. The maximum in monthly averaged clear-sky forcings was found in central China in February ($-18.49\ W\,m^{-2}$), whereas the minimum ($-0.51\ W\,m^{-2}$) occurred in south China in July. The largest all-sky forcing was $-2.60\ W\,m^{-2}$ in central China in January, whereas the smallest was $-0.16\ W\,m^{-2}$ in south China in July. Notably, the greatest difference between mean all-sky and clear-sky forcing values occurred in February in central China.

Fig. 8 shows the monthly mean clear- and all-sky DRFs over China (top panel) and the monthly mean total cloud cover from the ISCCP dataset (bottom panel). Variations of the mean DRF due to nitrate aerosols over China under clear- and all-sky conditions were similar: both minima occurred in July, with values of $-1.68\ W\,m^{-2}$ and $-0.40\ W\,m^{-2}$, respectively, but the maxima occurred in different months, namely February and January, with values of $-8.79\ W\,m^{-2}$ and $-1.38\ W\,m^{-2}$, respectively. This result can be explained

Table 2
Monthly and annual mean DRFs ($W\,m^{-2}$) due to nitrate aerosols at the TOA. For each month and region, the number on top is for the clear-sky case and the number below is for the all-sky case.

Region / Month	Central China	East China	North-east China	North China	Tibet Region	South-west China	South China	North-west China
1	−10.51	−7.63	−1.73	−2.69	−2.51	−6.49	−7.69	−2.62
	−2.60	−2.19	−0.61	−1.33	−0.87	−0.95	−1.59	−0.89
2	−18.49	−13.41	−2.67	−6.81	−2.93	−9.09	−13.08	−3.87
	−1.40	−1.13	−1.09	−2.43	−0.65	−1.09	−1.67	−0.66
3	−10.19	−7.08	−1.67	−4.24	−2.50	−8.18	−8.70	−2.07
	−1.24	−1.08	−0.57	−1.10	−0.59	−1.00	−0.78	−0.38
4	−7.63	−6.91	−4.66	−4.87	−3.06	−4.88	−5.42	−1.65
	−1.54	−1.39	−0.95	−1.01	−0.75	−0.77	−0.65	−0.43
5	−7.77	−5.39	−3.16	−4.02	−2.52	−2.79	−1.40	−2.02
	−0.90	−0.88	−0.57	−0.91	−0.56	−0.46	−0.31	−0.31
6	−4.78	−2.66	−2.03	−3.68	−2.50	−3.48	−1.16	−1.71
	−1.41	−0.75	−0.36	−0.82	−0.82	−0.67	−0.28	−0.34
7	−2.09	−1.41	−1.45	−1.94	−2.88	−1.66	−0.51	−1.52
	−0.62	−0.29	−0.20	−0.35	−0.80	−0.41	−0.16	−0.39
8	−6.78	−3.41	−0.98	−2.58	−3.65	−3.91	−1.58	−2.70
	−1.48	−0.70	−0.20	−0.44	−1.25	−0.94	−0.43	−0.63
9	−9.61	−4.80	−1.69	−3.80	−2.21	−5.32	−3.05	−2.77
	−2.02	−1.04	−0.48	−0.83	−0.85	−1.20	−0.81	−0.62
10	−10.15	−7.34	−2.12	−4.06	−2.11	−10.70	−8.24	−2.42
	−2.32	−1.69	−0.72	−1.31	−0.84	−1.57	−1.96	−0.43
11	−9.55	−7.12	−2.55	−3.73	−1.73	−7.26	−5.79	−2.14
	−1.92	−1.45	−0.79	−1.60	−1.00	−1.13	−1.44	−0.55
12	−4.85	−3.81	−0.96	−2.38	−2.78	−6.51	−3.90	−1.74
	−1.33	−1.10	−0.26	−0.79	−1.70	−1.09	−0.85	−0.72
Annual	−8.53	−5.92	−2.14	−3.73	−2.62	−5.86	−5.04	−2.27
	−1.57	−1.14	−0.57	−1.08	−0.89	−0.94	−0.91	−0.53

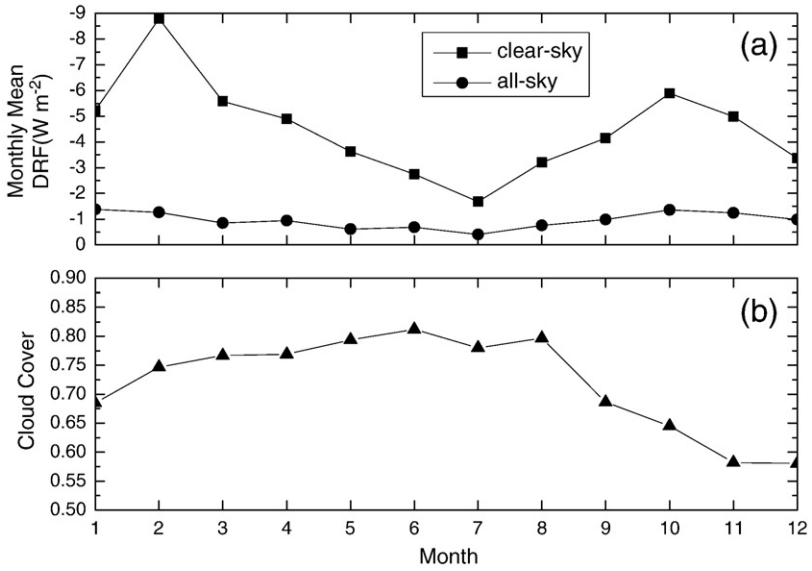

Fig. 8. Monthly mean DRFs under clear-sky and all-sky conditions over China (a) and (b) monthly mean total cloud cover from the ISCCP dataset.

by looking at the time series of monthly mean cloud cover, which is greater in February than in January, so greatly reduces the clear-sky forcing in February. Note that there is no simple linear correlation between all-sky DRFs and cloud cover because different cloud categories have different effects on radiative forcings. Other factors besides cloud cover can also affect the DRF, such as the cloud liquid water path, cloud droplet effective radius, and cloud thickness.

3.4. Error analysis of using sulfate optical properties to calculate DRF due to nitrate aerosols

The optical properties of sulfate aerosols have generally been used to calculate the DRF due to nitrate aerosols, which may lead to uncertainties in the estimated nitrate DRF. Here, we evaluate these uncertainties. The terms RF_{SO4} and RF_{NO3} represent DRFs due to nitrate aerosols that were calculated by using the optical properties of sulfate and nitrate, respectively. The difference between them, expressed as $\Delta = RF_{NO3} - RF_{SO4}$, is the absolute error in DRFs due to nitrate aerosols when sulfate optical properties are used in radiative transfer calculations. Fig. 9 shows the geographic distribution of absolute errors over China for the month of January for the all-sky case. All of the error values are positive, indicating that nitrate aerosol DRFs calculated using sulfate optical properties are less than those using the optical properties of nitrate. The maximum error was 0.16 W m^{-2}, which translates into an underestimation of the local radiative forcing by 6.2%, compared to the maximum regional forcing of −2.60 W m^{-2} in January (see Table 2).

4. Summary

In this paper, we estimated DRFs due to nitrate aerosols under clear- and all-sky conditions on the basis of the optical parameters of nitrate and discussed their seasonal variations

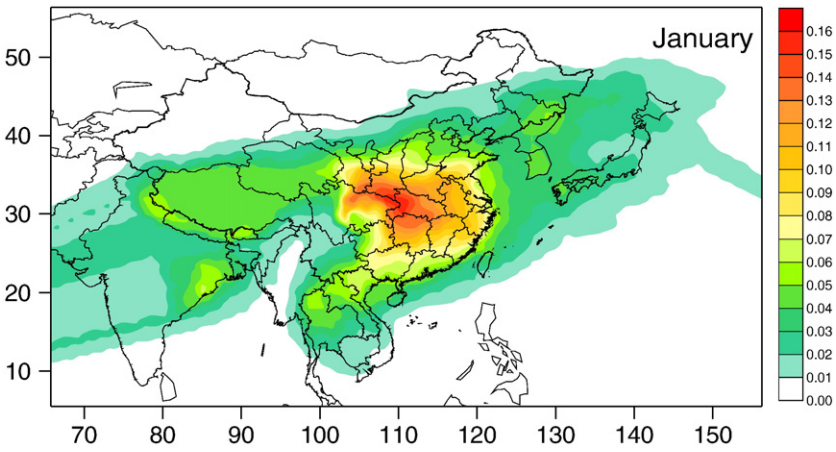

Fig. 9. Absolute errors in DRF due to nitrate aerosols caused by using the optical properties of sulfate aerosols for the calculation for all-sky condition. Units are in W m^{-2}.

over different areas of China. Our main conclusions are as follows.

Differences in the optical properties of nitrate and sulfate aerosols change with wavelength and/or relative humidity. Local forcings due to nitrate aerosols, calculated using sulfate optical properties, can be underestimated by up to 6.2%, according to this work. This brings about uncertainties, especially in regions with large emissions.

Nitrate forcings show significant seasonal variations over China, with seasonal mean all-sky forcings over China in spring, summer, autumn, and winter equal to $-0.80\ W\ m^{-2}$, $-0.61\ W\ m^{-2}$, $-1.20\ W\ m^{-2}$, and $-1.21\ W\ m^{-2}$, respectively. In April, for example, the largest DRFs were found in central China, with a monthly mean value of $-1.54\ W\ m^{-2}$ for the all-sky case, followed by DRFs in east China and north China, with monthly mean values of $-1.39\ W\ m^{-2}$ and $-1.01\ W\ m^{-2}$, respectively. This is not surprising because these regions are highly industrialized and generate more emissions. The lowest DRFs ($-0.43\ W\ m^{-2}$) occurred in northwest China, a remote and rural/desert-like region.

The seasonal and geographical distributions of DRFs due to nitrate aerosols are in general agreement with those of its column burdens. However, some discrepancies exist in some locations, and are probably caused by factors such as meteorological conditions, surface albedo, solar zenith angle, or the vertical distribution of the aerosol.

A comparison of clear-sky and all-sky cases shows that clouds can greatly reduce the DRF of nitrate aerosols. The annual mean DRF due to nitrate was $-4.51\ W\ m^{-2}$ over China under clear-sky conditions, whereas the magnitude was reduced by about 78.9% to $-0.95\ W\ m^{-2}$ in the all-sky case.

Finally, it should be noted that other factors, like the emission of nitrate aerosols and the uncertainty in HITRAN refractive indices of nitrated themselves, will also affect the estimation of its forcing. In this paper, we only discuss errors in DRF incurred by using its optical properties.

Acknowledgments

This work is financially supported by the National Basic Research Program of China (Grant Nos. 2011CB403405 and 2012CB955303), and the Public Meteorology Special Foundation of MOST (Grant no. GYHY200906020).

References

Adams, P.J., Seinfeld, J.H., Koch, D., Mickley, L., Jacob, D., 2001. General circulation model assessment of direct radiative forcing by the sulfate–nitrate–ammonium-water inorganic aerosol system. J. Geophys. Res. 106 (D1), 1097–1112.

An, J.L., Ueda, H., Wang, Z.F., Matsuda, K., Kajino, M., Cheng, X.J., 2002. Simulations of monthly mean nitrate concentrations in precipitation over East Asia. Atmos. Environ. 36 (26), 4159–4171.

Bergin, M.H., Cass, G.R., Xu, J., Fang, C., Zeng, L.M., Yu, T., Salmon, L.G., Kiang, C.S., Tang, X.Y., Zhang, Y.H., Chameides, W.L., 2001. Aerosol radiative, physical, and chemical properties in Beijing during June 1999. J. Geophys. Res. 106 (D16), 17969–17980.

Dentener, F., Kinne, S., Bond, T., Boucher, O., Cofala, J., Generoso, S., Ginoux, P., Gong, S., Hoelzemann, J.J., Ito, A., Marelli, L., Penner, J.E., Putaud, J.-P., Textor, C., Schulz, M., Van der Werf, G.R., Wilson, J., 2006. Emissions of primary aerosol and precursor gases in the years 2000 and 1750 prescribed datasets for AeroCom. Atmos. Chem. Phys. Discuss. 6, 2703–2763.

Diederen, H.S.M.A., Guicherit, R., Hollander, J.C.T., 1985. Visibility reduction by air pollution in The Netherlands. Atmos. Environ. 19, 377–383.

Han, X., Zhang, M.-G., Han, Z.-W., Xin, J.-Y., Wang, L.-L., Qiu, J.-H., Liu, Y.-J., 2010. Model analysis of aerosol optical depth distributions over East Asia. Sci. China, Ser. D Earth Sci. 53 (7), 1079–1090.

IPCC, 2007. Climate Change 2007: The Physical Science Basis. Contribution of Working Group I to the Fourth Assessment Report of the Intergovernmental Panel on Climate Change. In: Solomon, S., Qin, D., Manning, M., Chen, Z., Marquis, M., Averyt, K.B., Tignor, M., Miller, H.L. (Eds.), Cambridge University Press, Cambridge, United Kingdom and New York, NY, USA.

Lacis, A.A., Hansen, J.E., 1974. A parameterization for the absorption of solar radiation in the Earth's atmosphere. J. Atmos. Sci. 31, 118–133.

Li, Z., Chen, H., Cribb, M., Dickerson, R., Holben, B., Li, C., Lu, D., Luo, Y., Maring, H., Shi, G., Tsay, S., Wang, P., Wang, Y., Xia, X., Zheng, Y., Yuan, T., Zhao, F., 2007. Preface to special section on East Asian studies of tropospheric aerosols: an international regional experiment (EAST-AIRE). J. Geophys. Res. 112, D22S00, http://dx.doi.org/10.1029/2007JD008853.

Li, S., Wang, T.-J., Zhuang, B.-L., Han, Y., 2009. Indirect radiative forcing and climatic effect of the anthropogenic nitrate aerosol on regional climate of China. Adv. Atmos. Sci. 26 (3), 543–552.

Liao, H., Seinfeld, J.H., 2005. Global impacts of gas-phase chemistry aerosol interactions on direct radiative forcing by anthropogenic aerosols and ozone. J. Geophys. Res. 110, D18208.

Liao, H., Seinfeld, J.H., Adams, P.J., Mickley, L.J., 2004. Global radiative forcing of coupled tropospheric ozone and aerosols in a unified general circulation model. J. Geophys. Res. 109, D16207.

Liu, X., Wang, J., Christopher, S.A., 2003. Shortwave direct radiative forcing of Saharan dust aerosols over the Atlantic Ocean. Int. J. Remote. Sens. 24 (24), 5147–5160.

Myhre, C.E.L., Grothe, H., Gola, A.A., Nielsen, C.J., 2005. Optical constants of HNO_3/H_2O and $H_2SO_4/HNO_3/H_2O$ at low temperatures in the infrared region. J. Phys. Chem. A 109, 7166–7171.

Nakajima, T., Tsukamoto, M., Tsushima, Y., Numaguti, A., Kimura, T., 2000. Modeling of the radiative process in an atmospheric general circulation model. Appl. Opt. 39, 4869–4878.

Ohara, T., Akimoto, H., Kurokawa, J., Horii, N., Yamaji, K., Yan, X., Hayasaka, T., 2007. An Asian emission inventory of anthropogenic emission sources for the period 1980–2020. Atmos. Chem. Phys. 7, 4419–4444.

Pham, M., Boucher, O., Hauglustaine, D., 2005. Changes in atmospheric sulfur burdens and concentrations and resulting radiative forcings under IPCC SRES emission scenarios for 1990–2100. J. Geophys. Res. 110, D06112.

Quinn, P.K., Bates, T.S., 2005. Regional aerosol properties: comparisons from ACE 1, ACE 2, Aerosols99, INDOEX, ACE Asia, TARFOX, and NEAQS. J. Geophys. Res. 110, D14202.

Rossow, W.B., Schiffer, R.A., 1999. Advances in understanding clouds from ISCCP. Bull. Am. Meteorol. Soc. 80, 2261–2287.

Rothman, L.S., Jacquemart, D., Barbe, A., Chris Benner, D., Birk, M., Brown, L.R., Carleer, M.R., Chackerian, C., Chance, K., Coudert, L.H., Dana, V., Devi, V.M., Flaud, J.-M., Gamache, R.R., Goldman, A., Hartmann, J.-M., Jucks, K.W., Maki, A.G., Mandin, J.-Y., Massie, S.T., Orphal, J., Perrin, A., Rinsland, C.P., Smith, M.A.H., Tennyson, J., Tolchenov, R.N., Toth, R.A., Vander Auwera, J., Varanasi, P., Wagner, G., 2005. The HITRAN 2004 molecular spectroscopic database. J. Quant. Spectrosc. Radiat. Transfer 96 (2), 139–204.

Schiffer, R.A., Rossow, W.B., 1983. The International Satellite Cloud Climatology Project (ISCCP): The first project of the World Climate Research Programme. Bull. Am. Meteorol. Soc. 64, 779–784.

Streets, D.G., Waldhoff, S.T., 2000. Present and future emissions of air pollutants in China: SO_2, NO_x, and CO. Atmos. Environ. 34, 363–374.

Sun, J., Zhang, Q., Canagaratna, M., Zhang, Y., Ng, N., Sun, Y., Jayne, J., Zhang, X., Zhang, X., Worsnop, D., 2010. Highly time- and size-resolved characterization of submicron aerosol particles in Beijing using an aerodyne mass spectrometer. Atmos. Environ. 44, 131–140.

Tang, I.N., 1996. Chemical and size effects of hygroscopic aerosols on light and scattering coefficients. J. Geophys. Res. 101 (14), 19,245–19,250.

Ten Brink, H.M., Veefkind, J.P., van der Waijers-Ijpelaan, A., Hage, J.C., 1996. Aerosol light-scattering in The Netherlands. Atmos. Environ. 30 (24), 4251–4261.

Van Dorland, R., Dentener, F.J., Lelieveld, J., 1997. Radiative forcing due to tropospheric ozone and sulfate aerosols. J. Geophys. Res. 102 (D23), 28,079–28,100.

Wang, T.J., Min, J.Z., Xu, Y.F., Kase, L., 2003. Seasonal variations of anthropogenic sulfate aerosol and direct radiative forcing over China. Meteorol. Atmos. Phys. 84, 185–198.

Wang, T.J., Li, S., Shen, Y., Deng, J.J., Xie, M., 2010. Investigations on direct and indirect effect of nitrate on temperature and precipitation in China using a regional climate chemistry modeling system. J. Geophys. Res. 115, D00K26, http://dx.doi.org/10.1029/2009JD013264.

Wiscombe, W.J., 1980. Improved Mie scattering algorithms. Appl. Opt. 19 (9), 1505–1509.

World Meteorological Organization (WMO), 1983. Report of the experts meeting on aerosols and their climatic effects. World Meteorological Organization (WMO), Williamsburg, Virginia, p. 17.

Yamamoto, G., Tanaka, M., 1971. Increase of global albedo due to air pollution. J. Atmos. Sci. 29, 1405–1412.
Yang, Q., Fu, Q., Austin, J., Gettelman, A., Li, F., Vömel, H., 2008. Observationally derived and general circulation model simulated tropical stratospheric upward mass fluxes. J. Geophys. Res. 113, D00B07, http://dx.doi.org/10.1029/2008JD009945.
Zhang, H., Nakajima, T., Shi, G.Y., Suzuki, T., Imasu, R., 2003. An optimal approach to overlapping bands with correlated k distribution method and its application to radiative calculations. J. Geophys. Res. 108 (D20), 4641.
Zhang, H., Shi, G.Y., Nakajima, T., Suzuki, T., 2006a. The effects of the choice of k-interval number on radiative calculations. J. Quant. Spectrosc. Radiat. Transfer 98 (1), 31–43.
Zhang, H., Suzuki, T., Nakajima, T., Shi, G.Y., Zhang, X.Y., Liu, Y., 2006b. The effects of band division on radiative calculations. Opt. Eng. 45 (1), 016002.
Zhang, M.G., Gao, L.J., Ge, C., Xu, Y.P., 2007. Simulation of nitrate aerosol concentrations over East Asia with the model system RAMS-CMAQ. Tellus 59B, 372–380.
Zhang, H., Ma, J.H., Zheng, Y.F., 2009. A modeling study of global radiative forcing due to dust aerosol. Acta Meteorol. Sin. 67 (4), 510–521.
Zhang, Y., Zhang, X., Sun, J., Lin, W., Gong, S., Shen, X., Yang, S., 2011. Characterization of new particle and secondary aerosol formation during summertime in Beijing, China. Tellus B 63, 382–394.